

INCLINATION-DEPENDENT LUMINOSITY FUNCTION OF SPIRAL GALAXIES IN THE SLOAN DIGITAL SKY SURVEY: IMPLICATION FOR DUST EXTINCTION

ZHENGYI SHAO^{1,2}, QUANBAO XIAO^{1,2}, SHIYIN SHEN^{1,2}, H. J. MO³, XIAOYANG XIA⁴, ZUGAN DENG⁵

(Received; Accepted)
Draft version November 22, 2006

ABSTRACT

Using a samples of 61506 spiral galaxies selected from the SDSS DR2, we examine the luminosity function (LF) of spiral galaxies with different inclination angles. We find that the characteristic luminosity of the LF, L^* , decreases with increasing inclination, while the faint-end slope, α , depends only weakly on it. The inclination-dependence of the LF is consistent with that expected from a simple model where the optical depth is proportional to the cosine of the inclination angle, and we use a likelihood method to recover both the coefficient in front of the cosine, γ , and the LF for galaxies viewed face-on. The value of γ is quite independent of galaxy luminosity in a given band, and the values of γ obtained in this way for the 5 SDSS bands give an extinction curve which is a power law of wavelength ($\tau \propto \lambda^{-n}$), with a power index $n = 0.96 \pm 0.04$. Using the dust extinction for galaxies obtained by Kauffmann et al. (2003), we derive an ‘extinction-corrected’ luminosity function for spiral galaxies. Dust extinction makes M^* dimmer by about 0.5 magnitudes in the z -band, and about 1.2 magnitudes in the u -band. Since our analysis is based on a sample where selection effects are well under control, the dimming of edge-on galaxies relative to face-on galaxies is best explained by assuming that galaxy disks are optically thick in dust absorptions.

Subject headings: galaxies: spiral — galaxies: luminosity function — ISM: dust, extinction

1. INTRODUCTION

Dust plays an important role in the observed properties of galaxies. It not only causes galaxies to dim but also causes them to redden. In order to obtain the intrinsic properties of galaxies from observation, it is necessary to understand dust extinction. Dust extinction is believed to be more important in late-type spiral galaxies than in early-type galaxies, since spiral galaxies are richer in cold gas and have on-going star formation (e.g. Calzetti 2001 for a review and references therein). Dust opacity in spiral disks can be probed by studying the average photometric properties of spiral galaxies as a function of disk inclination angle, as first suggested by Holmberg (1958, 1975). Theoretically, it can be shown that, for completely opaque disks, the surface brightness to be observed is almost independent of inclination angle, while the luminosity dims as the inclination angle changes from face-on to edge-on. On the other hand, for completely transparent disks, the luminosity is independent of inclination while the surface brightness brightens as the disk changes from face-on to edge-on. However, the power of the Holmberg test is limited by the finite sizes of galaxy samples, because it is in general difficult to accurately estimate the inclination angles for individual galaxies. The axis ratios of galaxy images are usually used to estimate the inclination angles. For an infinitesimally thin

and round disk, the inclination angle θ can be obtained directly from the axis ratio b/a through $\cos \theta = b/a$. Unfortunately, real disks are neither completely round nor infinitesimally thin, and the observed axis ratio depends not only on the inclination angle but also on the ellipticity and thickness of the galaxy. Unless such dependence is fully taken into account, the results from the Holmberg test cannot be interpreted straightforwardly. In addition, the test based on the average photometric properties of galaxies as functions of inclination angle may be further complicated by the incompleteness and selection bias of galaxy sample. For example, if disk galaxies are optically thin, a galaxy sample may be biased for low-luminosity galaxies with high inclinations because of the enhanced surface brightness. With such selection bias, face-on galaxies will on average be brighter than edge-on galaxies, which may be falsely interpreted as the disks being optically thick. Because of these limitations, the conclusion about the opacity of the disk galaxies are still controversial (e.g. Burstein Haynes & Faber 1991; Byun 1993; Giovanelli et al. 1994, 1995; Xilouris et al. 1999; Masters, Giovanelli & Haynes 2003; Holwerda et al. 2005).

With a large and well-defined sample, the above-mentioned difficulties in the Holmberg test can in principle be overcome. As shown in Ryden (2004), a large sample allows one to estimate the thickness and ellipticity robustly from the distribution of axis ratios in a statistical way. Moreover, with a large, well-defined sample, one can study the conditional distribution functions of photometric properties for given inclination angles, instead of just considering the mean photometric properties of galaxies. Thus, the selection bias and sample incompleteness can be taken into account strictly in a statistical sense. With the advent of the Sloan Digital Sky Survey (SDSS, York et al. 2000), it is now possible to make such analysis.

¹ Shanghai Astronomical Observatory, CAS, Shanghai 200030, P.R. China

² Joint institute for galaxy & cosmology, CAS, Shanghai 200030, P.R. China

³ Astronomy Department, University of Massachusetts, Amherst MA 01003, USA

⁴ Department of Physics, Tianjin Normal University, Tianjin 300074, P. R. China

⁵ Graduate School, Chinese Academy of Sciences, Beijing 100080, P. R. China

Electronic address: zyshao@shao.ac.cn

In this paper, we use the SDSS galaxy sample to study dust extinctions in spiral galaxies. Our analysis is based on the luminosity function (hereafter LF) of galaxies as a function of inclination angles. We statistically correct the axis ratios of galaxy images to obtain their inclination angles based on the method of Ryden (2004). We compare the change of LF with inclination angle in different wavebands to constrain the shape of the dust extinction curve. The paper is organized as follows. The selection of sample is described in § 2.1 and quantities to specify the inclinations of galaxies are discussed in § 2.2. In § 3, after a brief description of the LF estimators adopted in this paper (§ 3.1), we present the results of the LFs in all the 5 SDSS bands for galaxies of different inclination angles (§ 3.2). In § 4, the inclination-dependence of the LF is modelled in terms of dust extinction. The possible luminosity dependence of the dust extinction and the dust-corrected LF of spiral galaxies are discussed in § 5. Finally, our results are summarized in § 6.

2. OBSERVATIONAL DATA

2.1. Galaxy samples

The galaxy samples we used were selected from the New York University Value-Added Galaxy Catalog (NYU-VAGC, Blanton et al., 2005) of the SDSS second data release (DR2, Abazajian et al. 2004). The redshift catalog of the DR2 covers $2,627 \text{ deg}^2$ of the celestial sphere and photometric data in the 5 SDSS wave bands, u , g , r , i and z , are available for each of the galaxies (Abazajian et al. 2004) directly from the SDSS pipeline. The NYU-VAGC includes additional information for extragalactic targets, such as K -correction, spectroscopic target completeness, etc.. From the NYU-VAGC, we select spiral galaxies with $fracdeV_r \leq 0.5$, where the photometric parameter $fracdeV$ is a point spread function (PSF) corrected indicator of galaxy morphology. In the SDSS pipeline, each galaxy was fitted by an exponential profile and a de Vaucouleurs' profile. The best linear combination of these two profiles was used to represent the profile of the galaxy, and $fracdeV$ is the fraction of luminosity contributed by the de Vaucouleurs' profile. Bernardi et al. (2005) used $fracdeV_r \geq 0.8$ to select early-type galaxies. We use $fracdeV_r \leq 0.5$ to ensure that the galaxies we select are dominated by the exponential component.

To construct samples to study the LFs of galaxies, both redshift and flux limits are applied. Only galaxies with redshift in the range $0.01 \leq z_{\text{red}} \leq 0.22$ are selected. The upper limit is imposed to minimize the uncertainty in the K -correction and possible redshift evolutions of galaxies; the lower limit is employed to avoid the nearest galaxies with large uncertainties of distance caused by peculiar velocities. A flux limit in r band, $m_r = 17.60$, is chosen to ensure the completeness in spectroscopy. For other wave bands, the flux limits are chosen to be sufficiently high, so that almost all of the galaxies (99%) brighter than the limit in the band in consideration have r -band flux brighter than 17.60 mag. The flux limits of all 5 bands we use and the numbers of galaxies in the corresponding samples are listed in Table 1. Note that we use the Petrosian (1976) magnitude to refer the luminosities of galaxies. This definition of magnitude has the advantage that it is a uniform measurement of flux quite independent of the distance of the target. Furthermore,

TABLE 1
THE SAMPLE OF GALAXIES IN EACH SDSS BAND

Band	Flux Limit	Redshift Limit	N_{gal}	N_{spiral}
u	$14.50 < m < 18.60$	$0.01 < z < 0.22$	42033	24106
g	$14.50 < m < 17.90$	$0.01 < z < 0.22$	93221	43252
r	$14.50 < m < 17.60$	$0.01 < z < 0.22$	162279	61506
i	$14.50 < m < 17.15$	$0.01 < z < 0.22$	148934	52336
z	$14.50 < m < 16.85$	$0.01 < z < 0.22$	136151	43653

N_{gal} is the number of galaxies selected within the flux and redshift limits. N_{spiral} is the number of spiral galaxies selected with $fracdeV_r \leq 0.5$.

for an exponential profile the Petrosian magnitude contains almost all of the flux of the source (e.g. Stoughton et al. 2002).

For each band, the absolute magnitude M is calculated using

$$M_\lambda = m_\lambda - 5 \log(d_L/10pc) - K_\lambda(z) \quad (1)$$

where λ is the wave band in consideration, m_λ is the apparent magnitude corrected for Galactic extinction based on the $E(B - V)$ maps of Schlegel, Finkbeiner & Davis (1998), d_L is the luminosity distance, and $K_\lambda(z)$ is the K -correction value taken from NYU-VAGC. Throughout the paper, we use the standard Λ -cosmology with $\Omega_0 = 0.3$, $\Omega_\Lambda = 0.7$ and $H_0 = 100h^{-1} \text{ kms}^{-1} \text{ Mpc}$.

2.2. Inclination parameters

The apparent axis ratio of the image of a galaxy, which is provided by the SDSS pipeline, is a direct measurement of the inclination of spiral galaxies. If disks are thin and round, the minor-to-major axis ratio b/a is related to the inclination angle θ (defined to be the angle between the line-of-sight and the axis of angular momentum of the disk) by $b/a = \cos\theta$. In this paper, we use the r band axis ratio ab_exp_r , taken from the best fit of the images of galaxies with an exponential profile convolved with the PSF (see Stoughton et al. 2002). Since the sample galaxies we selected are expected to be dominated by the exponential component ($fracdeV_r \leq 0.5$), the parameter ab_exp_r (hereafter referred to as b/a) should be a reasonable representation of the apparent axis ratio.

Figure 1 shows the distribution of b/a for the sample galaxies (solid line). If disks are completely round and infinitesimally thin, and if their rotation axes are randomly orientated in space, the distribution of b/a should be flat. For our sample, the distribution is almost flat for $0.3 < b/a < 0.9$, but disks with axis ratios close to 1 or close to 0 are less common. The lack of very round images ($b/a \sim 1$) is caused by the intrinsic ellipticity, ϵ , of spiral galaxies, as demonstrated in detail by Ryden (2004). The lack of images with small b/a is caused by two factors. The first is the intrinsic thickness of galaxy disks: the typical scale height of a disk is about 10% of the disk scale length, as shown in Giovanelli et al. (1994). The other is the existence of a central bulge which, being spheroidal, can thicken the image of a spiral galaxy, especially an edge-on spiral. In what follows, we do not distinguish these two different causes of disk thickening. Instead we use a single 'effective thickness' parameter, ν , defined as the ratio of scale height to scale length, to represent the thickness of a spiral galaxy.

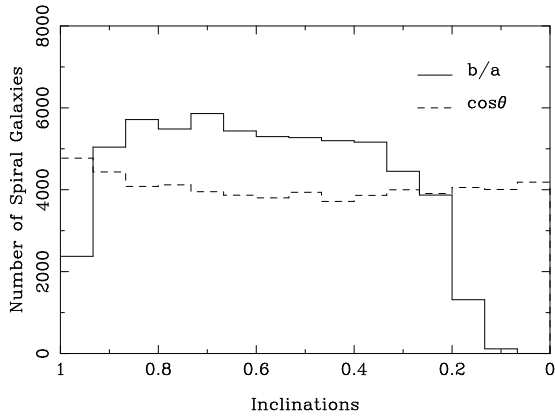


FIG. 1.— The distributions of the apparent axis ratio b/a (solid line) and of the simulated inclinations $\cos\theta$ (dashed line).

Using a sample of SDSS spiral galaxies that have relative large apparent size, $R_e > 5\sqrt{T_{\text{psf}}}$, where R_e is the effective radius of an exponential profile and T_{psf} is the adaptive second moment of the PSF image (so that $\sqrt{T_{\text{psf}}}$ may be used as a characteristic scale of the PSF), Ryden (2004) found that both ν and $\log\epsilon$ have roughly Gaussian distributions. For example, in the r -band, Ryden (2004) found that the median (ν_0) and dispersion (σ_ν) of the ν -distribution are 0.216 and 0.056, respectively, while those for the $\log\epsilon$ -distribution are $\log\epsilon_0 = -1.83$ and $\sigma_{\log\epsilon} = 0.93$. However, with a typical PSF of 1.5 arcsec, the majority of SDSS galaxies have $R_e < 5\sqrt{T_{\text{psf}}}$ (e.g. Shen et al. 2003). Moreover, the apparent thickness is expected to vary with the apparent size (R_e), with smaller images appearing rounder, even though the images are de-convolved with the PSF. Galaxies with small apparent sizes include not only intrinsically small galaxies at small distances, but also intrinsically luminous galaxies at large distances. Since the average bulge-to-disk ratio of spiral galaxies increases with galaxy luminosity, the bulge components may become more dominant in a sample that contains more distant galaxies with small apparent sizes. Furthermore the bulge components are in general easier to observe than the disk components, because of their higher surface brightness. Both factors will cause the distant, apparently small spirals to be rounder. For this reason, we divide our sample into subsamples according to the apparent sizes (R_e) of galaxies, and study the thickness parameter separately for each of the subsamples.

We assume that both the thickness parameter ν and ellipticity $\log\epsilon$ follow Gaussian distributions and estimate the thickness parameters ν_0 and σ_ν for spirals with different apparent sizes using the following Monte-carlo procedure. For a given galaxy with given shape parameters (ν and ϵ) and viewing angles (θ, φ), the apparent axis ratio b/a can be calculated using

$$b/a = \left[\frac{A + C - \sqrt{(A - C)^2 + B}}{A + C + \sqrt{(A - C)^2 + B}} \right]^{1/2}, \quad (2)$$

where

$$A = [1 - \epsilon(2 - \epsilon) \sin^2 \varphi] \cos^2 \theta + \nu^2 \sin^2 \theta, \quad (3)$$

$$B = 4\epsilon^2(2 - \epsilon)^2 \cos^2 \theta \sin^2 \varphi \cos^2 \varphi, \quad (4)$$

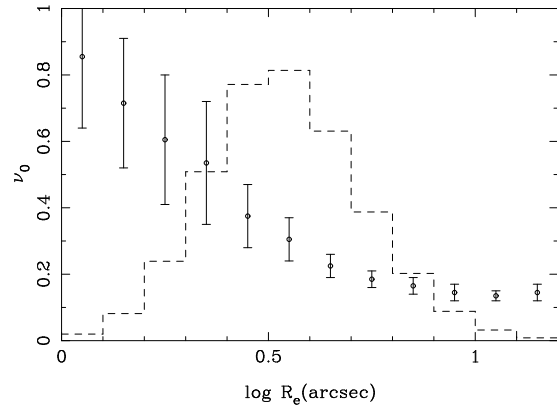


FIG. 2.— The best-fit values of the effective thickness parameters ν_0 and σ_ν (shown as error bars) for spiral galaxies with different apparent size $\log R_e$ in the r -band. Dashed line is the distribution of $\log R_e$ for sample galaxies.

$$C = 1 - \epsilon(2 - \epsilon) \cos^2 \varphi \quad (5)$$

(see Binney 1985). Model galaxies are assumed to have random distribution in the view angle, and to have random distributions in ν and $\log\epsilon$ according to their Gaussian distribution functions. To reduce model parameters, we assume that $\log\bar{\epsilon}$ and $\sigma_{\log\epsilon}$ have the values given by Ryden (2004). The best values of $\bar{\nu}$ and σ_ν are obtained by matching the predicted b/a distribution with the observed b/a distribution (for each R_e -subsample), with the use of the least-square criterion. The fitting results for ν_0 and σ_ν are plotted in Figure 2. As expected, disk galaxies with large apparent sizes have smaller ‘effective thickness’. At apparent size $R_e > 8$ arcsec, ν_0 reaches a constant value ~ 0.14 . This value may be considered as the upper limit of the effective thickness of the disks, or be explained as the intrinsic thickness of pure disk should be less than 0.14. Since the typical seeing condition in SDSS has $T_{\text{psf}} = 4\text{Pixel}^2$, the galaxies selected by Ryden (2004) have $R_e > 5\sqrt{T_{\text{psf}}}$ and so are dominated by galaxies with $R_e \gtrsim 4$ arcsec (see Figure 2). Our results for galaxies with $R_e \gtrsim 4$ arcsec are $\nu_0 \pm \sigma_\nu \sim 0.195 \pm 0.035$, close to the results of Ryden 0.216 ± 0.056 .

The above procedure also provides a statistical way to relate the real inclination of a galaxy (represented by $\cos\theta$) to the apparent axis ratio (b/a). To do this, each galaxy is assigned a possible viewing angle using a Monte Carlo method. For a galaxy with given (observed) b/a and R_e , we first randomly select a set of shape parameters (ν and ϵ) from their Gaussian distributions obtained above, and then calculate the apparent axis ratio using equation (2). The value of θ that best reproduces the observed b/a is taken to be the viewing angle of this galaxy. Since our samples are sufficiently large, the simulated values of θ should represent the real distribution of the inclination angles in a statistical sense.

Figure 3 shows the correlation between the simulated $\cos\theta$ and the observed b/a . The whole sample is divided into 15 subsets in b/a , with each subset containing a similar number of galaxies. In the figure, points are median values while errorbars are the 16-84 percentiles of the distribution. The distribution of $\cos\theta$ is also plotted in Figure 1 as the dashed lines. As one can see, $\cos\theta$ follows a nearly flat distribution as expected. However, it should

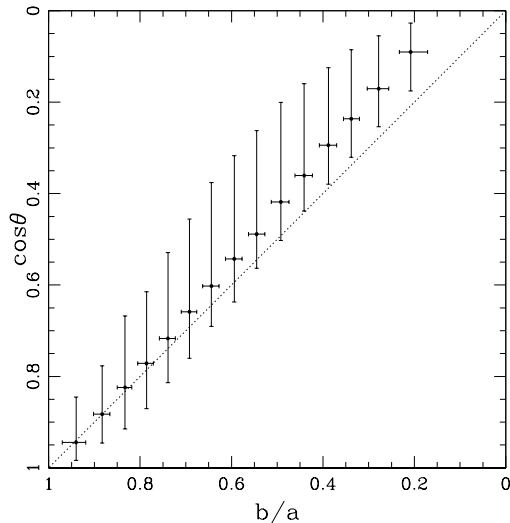


FIG. 3.— The correlation between the apparent axis ratio b/a and the simulated inclination $\cos\theta$. Points are located at the median value of b/a and $\cos\theta$, and error bars represent the 16-84 percentiles of the distribution.

be emphasized that $\cos\theta$ is an inclination parameter that has only statistical meaning. For individual galaxies, the uncertainty in $\cos\theta$ is as large as the scatter shown in Figure 3.

3. GALAXY LUMINOSITY FUNCTION: DEPENDENCE ON INCLINATION

3.1. Luminosity function estimator

In estimating the luminosity function (LF) of galaxies, we use the maximum-likelihood method proposed by Sandage, Tammann & Yahil (1979, hereafter STY). This method assumes that the LF of galaxies has the Schechter form (Schechter 1976),

$$\phi(L)dL = \phi^*(L/L^*)^\alpha \exp(-L/L^*)d(L/L^*), \quad (6)$$

where L^* is the characteristic luminosity, α the faint-end slope, and ϕ^* the overall amplitude of the LF. The STY method uses such a luminosity function to calculate the probability for a galaxy with luminosity L_i and redshift z_i to be included in a magnitude-limited sample:

$$p_i = \frac{\phi(L_i)dL}{\int_{L_{\min}(z_i)}^{L_{\max}(z_i)} \phi(L)dL}, \quad (7)$$

where $L_{\min}(z_i)$ and $L_{\max}(z_i)$ are the lowest and highest luminosities that a galaxy at redshift z_i can have in order for it to be included in the sample. The likelihood function is defined as

$$\mathcal{L} = \prod_i p_i \quad (8)$$

where the product extends over all galaxies in the sample, and its maximization provides an estimate for α and L^* (or equivalently the corresponding absolute magnitude M^*).

We estimate the LFs for spiral galaxies with different inclinations in all the 5 SDSS bands. In order to make meaningful comparisons among the results, only galaxies

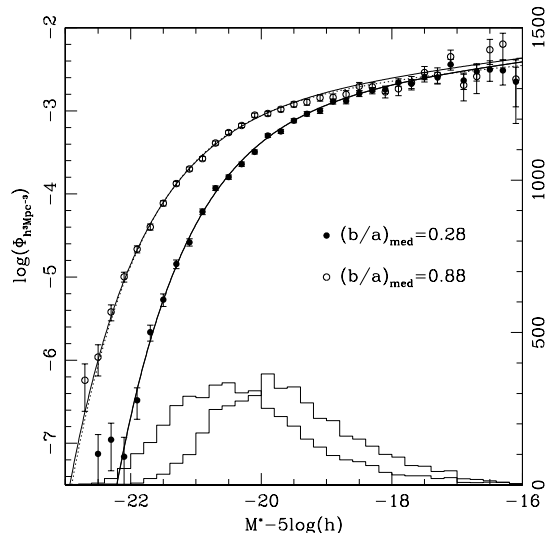


FIG. 4.— The luminosity functions for the nearly face-on subsample (open circles) and the nearly edge-on subsample (solid circles). Smooth curves are the luminosity functions obtained using the STY method. Dotted curves show the best fit of the data points with a Schechter function. Solid curves are the fit results assuming $\alpha = \langle\alpha_{\text{sub}}\rangle = -1.25$. Points and errors are obtained from the SWML method. Histograms near the bottom are the numbers of galaxies in bins of absolute magnitude. The results for edge-on galaxies are shifted vertically by a factor of two for easy to compare the shape of LFs.

in the luminosity range from $M^* + 3.5$ to $M^* - 2.0$ are used. In practice, an initial value of M^* was chosen and an iterative procedure was used to determine M^* and other LF parameters. Some extreme bright galaxies are rejected automatically by this selection.

As comparison, we also estimate each LF using the step-wise maximum-likelihood (SWML) method of Efstathiou et al. (1988). Here the LF is represented by a non-parametric step function and the maximization of the likelihood function is used to determine the relative amplitudes at all the steps.

3.2. Results

In Table 2 we list the fitting parameters of the LFs of spiral galaxies in the 5 SDSS bands, using the STY method. SWML method gives similar results; they are not presented here in order to save space. The subscript 'obs' in α_{obs} and M_{obs}^* denote that these are derived directly from observational data, to distinguish them from the quantities for other LFs discussed in this paper. Comparing the results with that obtained by Blanton et al. (2001), for all SDSS galaxies, we see that our LFs are steeper in the faint end (i.e. α is more negative) in all 5 bands. This is consistent with the fact that the faint-end slope for late-type galaxies is steeper than that for early types (Nakamura et al. 2003). In addition, the typical color of galaxies in our sample, as represented by the values of M_{obs}^* in the 5 bands is bluer than for the total sample, as is expected from the fact that spiral galaxies are on average bluer than early-type galaxies. To study the dependence of the LF on galaxy inclinations, we divide sample of each band into 15 subsamples according to the apparent axis ratio b/a in the r band (see § 2.2

TABLE 2
PARAMETERS OF LUMINOSITY FUNCTION FOR SPIRAL GALAXIES IN
EACH OF THE 5 SDSS BANDS

Band	N_{spiral}	α_{obs}	M_{obs}^*
<i>u</i>	23757	-1.47 ± 0.02	-18.32 ± 0.02
<i>g</i>	42620	-1.36 ± 0.01	-19.60 ± 0.01
<i>r</i>	60523	-1.34 ± 0.01	-20.26 ± 0.01
<i>i</i>	51593	-1.36 ± 0.01	-20.62 ± 0.01
<i>z</i>	43030	-1.31 ± 0.01	-20.74 ± 0.01

and Figure 3 for details). LF is estimated for each of the subsamples in each of the 5 SDSS wave bands. As an example, Figure 4 shows the LFs for two extreme subsamples, one for nearly edge-on galaxies, and the other for nearly face-on galaxies, in the *r*-band. Note that the results obtained from the SWML method (open and solid circles) match extremely well with those obtained from the STY method (solid lines), showing that the Schechter function is a valid assumption for the LFs for spiral galaxies with different inclinations. Clearly, both subsamples have similar α , but edge-on galaxies are systematically fainter than face-on galaxies, by about ~ 0.65 magnitude. In Table 3, we list the LF parameters obtained from the SYT method for all the inclination subsamples, and we use the subscript 'sub' to denote the parameters for subsamples. The changes of α_{sub} and M_{sub}^* with b/a are also plotted in Figure 5 and in the left panel of Figure 6, respectively. There is a systematic change of M_{sub}^* , with face-on galaxies having a brighter characteristic magnitude than edge-on galaxies. This change of M_{sub}^* with inclination becomes smoother if we fix the faint-end slope α to be the average value of the 15 subsamples (dotted lines in Figure 5), as one can see from the right panel of Figure 6. These values are denoted as $M_{\text{sub},2}^*$ and also listed in Table 3. In addition, the inclination-dependence of M_{sub}^* is stronger in blue band, as is expected if the dependence is caused by dust extinction.

A systematic change of α with b/a is expected if dust extinction depends on galaxy luminosity for $L < L^*$. The absence of any strong systematic dependence of α on b/a in the data suggests that dust extinction does not depend on galaxy luminosity strongly, at least for sub- L^* galaxies. Note, however, that the dust extinction considered here is relative to that for face-on galaxies. If dust extinction in face-on galaxies depends strongly on luminosity, then a strong luminosity-dependent dust extinction cannot be excluded. We will discuss this in more detail in § 5.1.

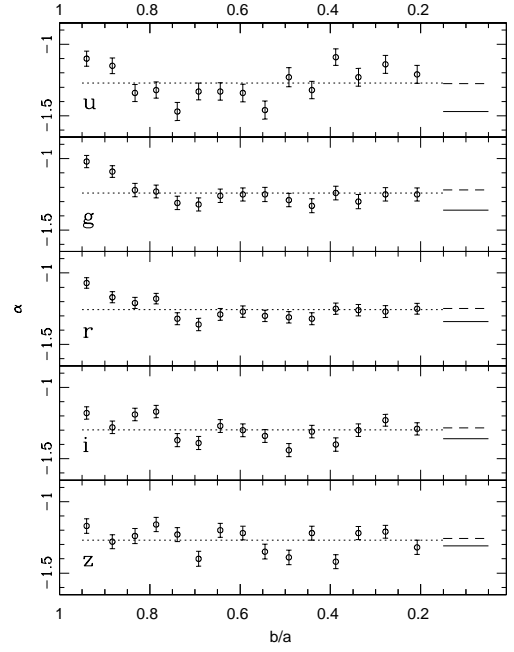


FIG. 5.— The dependence of the faint-end slope of the LF, α , on the axis ratios of galaxies (b/a). Dotted lines for $\langle\alpha_{\text{sub}}\rangle$ of table 3; Solid lines for α_{obs} of table 2; Dashed line for α_0 of table 5 (see § 4.1).

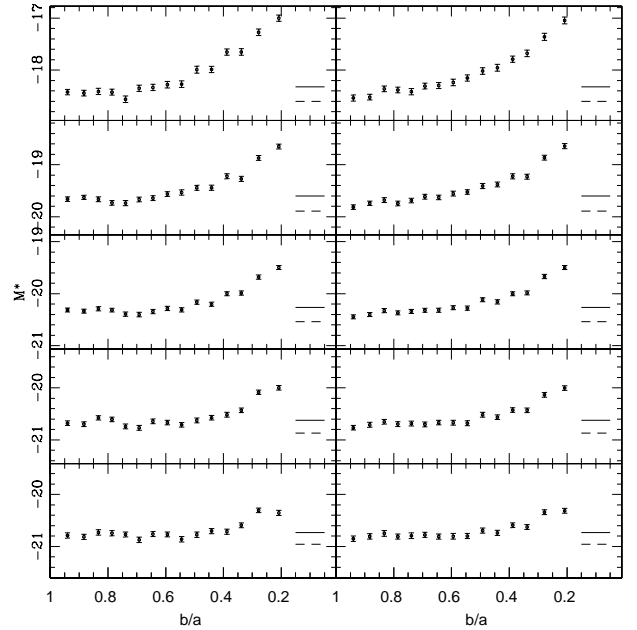


FIG. 6.— The dependence of the characteristic magnitude of the LF, M^* , on the axis ratios of galaxies (b/a). In the left panel, the values of M^* are taken from the fit with both M^* and α as free parameters. In the right panel, the values of M^* are obtained from the fit assuming $\alpha = \langle\alpha_{\text{sub}}\rangle$. Solid lines for M_{obs}^* of table 2; Dashed line for M_0 of table 5 (see § 4.1).

TABLE 3
LUMINOSITY FUNCTION PARAMETERS FOR SPIRAL GALAXIES WITH
DIFFERENT INCLINATIONS.

Band	$N_{\text{sub},1}$	$(b/a)_{\text{med}}$	$(\cos\theta)_{\text{med}}$	α_{sub}	$M_{\text{sub},1}^*$	$N_{\text{sub},2}$	$\langle\alpha_{\text{sub}}\rangle$	$M_{\text{sub},2}^*$
<i>u</i>	1256	0.21	0.09	-1.21±0.09	-17.00±0.06	1260	-1.27	-17.04±0.06
	1216	0.28	0.17	-1.14±0.08	-17.27±0.06	1223	.	-17.36±0.07
	1373	0.34	0.24	-1.23±0.08	-17.65±0.06	1374	.	-17.68±0.06
	1440	0.39	0.29	-1.09±0.07	-17.65±0.06	1451	.	-17.79±0.06
	1519	0.44	0.36	-1.32±0.07	-17.99±0.07	1516	.	-17.95±0.06
	1544	0.49	0.42	-1.23±0.07	-17.99±0.06	1545	.	-18.02±0.06
	1658	0.55	0.49	-1.46±0.07	-18.27±0.07	1657	.	-18.15±0.06
	1604	0.59	0.54	-1.34±0.07	-18.28±0.06	1606	.	-18.24±0.07
	1672	0.64	0.60	-1.33±0.07	-18.33±0.06	1672	.	-18.30±0.06
	1685	0.69	0.66	-1.33±0.07	-18.35±0.06	1685	.	-18.31±0.05
	1665	0.74	0.72	-1.47±0.07	-18.56±0.07	1664	.	-18.41±0.07
	1750	0.79	0.77	-1.32±0.07	-18.42±0.06	1746	.	-18.38±0.05
	1709	0.83	0.82	-1.34±0.07	-18.41±0.06	1705	.	-18.36±0.06
	1765	0.88	0.88	-1.15±0.06	-18.44±0.06	1769	.	-18.52±0.06
	1860	0.94	0.94	-1.10±0.06	-18.42±0.05	1870	.	-18.54±0.05
<i>g</i>	2672	0.21	0.09	-1.25±0.05	-18.65±0.05	2671	-1.24	-18.64±0.05
	2598	0.28	0.17	-1.25±0.05	-18.87±0.05	2598	.	-18.86±0.05
	2726	0.34	0.24	-1.30±0.05	-19.27±0.05	2726	.	-19.23±0.05
	2788	0.39	0.29	-1.24±0.05	-19.22±0.04	2788	.	-19.22±0.05
	2841	0.44	0.36	-1.33±0.05	-19.44±0.05	2842	.	-19.38±0.04
	2834	0.49	0.42	-1.29±0.05	-19.44±0.05	2834	.	-19.41±0.05
	2894	0.55	0.49	-1.25±0.05	-19.53±0.05	2897	.	-19.52±0.04
	2853	0.59	0.54	-1.25±0.05	-19.56±0.05	2852	.	-19.56±0.05
	2887	0.64	0.60	-1.26±0.05	-19.65±0.05	2889	.	-19.63±0.04
	2921	0.69	0.66	-1.32±0.05	-19.67±0.05	2920	.	-19.61±0.05
	2897	0.74	0.72	-1.31±0.05	-19.74±0.05	2896	.	-19.69±0.04
	2925	0.79	0.77	-1.23±0.05	-19.74±0.05	2926	.	-19.75±0.05
	2839	0.83	0.82	-1.22±0.05	-19.66±0.05	2838	.	-19.68±0.04
	3008	0.88	0.88	-1.09±0.05	-19.63±0.04	3014	.	-19.74±0.04
	2981	0.94	0.94	-1.02±0.05	-19.66±0.04	2983	.	-19.82±0.04
<i>r</i>	4093	0.21	0.09	-1.25±0.04	-19.50±0.04	4093	-1.25	-19.50±0.04
	4075	0.28	0.17	-1.27±0.04	-19.68±0.04	4075	.	-19.67±0.04
	4047	0.34	0.24	-1.26±0.04	-19.99±0.04	4048	.	-19.98±0.04
	4026	0.39	0.29	-1.25±0.04	-20.00±0.04	4027	.	-20.00±0.04
	4011	0.44	0.36	-1.32±0.04	-20.20±0.04	4010	.	-20.16±0.04
	4092	0.49	0.42	-1.31±0.04	-20.16±0.04	4089	.	-20.11±0.04
	3987	0.55	0.49	-1.30±0.04	-20.31±0.04	3988	.	-20.28±0.04
	3987	0.59	0.54	-1.27±0.04	-20.28±0.04	3987	.	-20.27±0.04
	4072	0.64	0.60	-1.29±0.04	-20.34±0.04	4071	.	-20.32±0.04
	4042	0.69	0.66	-1.36±0.04	-20.40±0.04	4043	.	-20.32±0.04
	4030	0.74	0.72	-1.32±0.04	-20.39±0.04	4033	.	-20.34±0.04
	4061	0.79	0.77	-1.18±0.04	-20.32±0.04	4059	.	-20.37±0.04
	3979	0.83	0.82	-1.21±0.04	-20.29±0.04	3983	.	-20.33±0.04
	4081	0.88	0.88	-1.17±0.04	-20.34±0.04	4085	.	-20.40±0.04
	4014	0.94	0.94	-1.07±0.04	-20.31±0.04	4016	.	-20.44±0.04
<i>i</i>	3700	0.21	0.09	-1.29±0.04	-20.00±0.04	3700	-1.30	-20.00±0.04
	3603	0.28	0.17	-1.23±0.05	-20.08±0.04	3604	.	-20.13±0.04
	3585	0.34	0.24	-1.30±0.05	-20.43±0.04	3585	.	-20.43±0.05
	3543	0.39	0.29	-1.40±0.05	-20.52±0.05	3546	.	-20.43±0.04
	3456	0.44	0.36	-1.31±0.05	-20.57±0.05	3456	.	-20.56±0.04
	3503	0.49	0.42	-1.44±0.05	-20.62±0.05	3500	.	-20.52±0.05
	3394	0.55	0.49	-1.34±0.05	-20.71±0.04	3393	.	-20.68±0.05
	3364	0.59	0.54	-1.30±0.05	-20.67±0.05	3365	.	-20.67±0.05
	3401	0.64	0.60	-1.27±0.05	-20.64±0.04	3402	.	-20.67±0.04
	3332	0.69	0.66	-1.39±0.05	-20.77±0.05	3336	.	-20.70±0.05
	3355	0.74	0.72	-1.37±0.05	-20.74±0.05	3355	.	-20.69±0.05
	3385	0.79	0.77	-1.17±0.05	-20.61±0.04	3387	.	-20.70±0.04
	3270	0.83	0.82	-1.19±0.05	-20.58±0.04	3269	.	-20.65±0.04
	3381	0.88	0.88	-1.28±0.05	-20.70±0.05	3379	.	-20.71±0.05
	3338	0.94	0.94	-1.18±0.05	-20.68±0.04	3335	.	-20.77±0.04
<i>z</i>	3275	0.21	0.09	-1.32±0.05	-20.35±0.05	3273	-1.27	-20.31±0.05
	3229	0.28	0.17	-1.21±0.05	-20.31±0.05	3233	.	-20.34±0.04
	3147	0.34	0.24	-1.22±0.05	-20.59±0.05	3147	.	-20.63±0.05
	3086	0.39	0.29	-1.42±0.05	-20.72±0.05	3076	.	-20.59±0.05
	2928	0.44	0.36	-1.22±0.06	-20.70±0.05	2929	.	-20.74±0.05
	2934	0.49	0.42	-1.39±0.06	-20.77±0.05	2932	.	-20.69±0.05
	2859	0.55	0.49	-1.35±0.06	-20.86±0.05	2857	.	-20.80±0.05
	2724	0.59	0.54	-1.22±0.06	-20.77±0.05	2724	.	-20.80±0.05
	2775	0.64	0.60	-1.20±0.06	-20.76±0.05	2778	.	-20.81±0.05
	2755	0.69	0.66	-1.40±0.06	-20.87±0.05	2752	.	-20.78±0.05
	2640	0.74	0.72	-1.23±0.06	-20.77±0.05	2641	.	-20.80±0.05
	2704	0.79	0.77	-1.16±0.06	-20.75±0.05	2706	.	-20.81±0.05
	2603	0.83	0.82	-1.24±0.06	-20.73±0.05	2604	.	-20.75±0.05
	2682	0.88	0.88	-1.28±0.06	-20.81±0.05	2684	.	-20.81±0.05
	2705	0.94	0.94	-1.17±0.06	-20.79±0.05	2706	.	-20.85±0.05

Samples of all 5 bands are divided into 15 sub-samples by b/a , while $(b/a)_{\text{med}}$ and $(\cos\theta)_{\text{med}}$ show the median values of inclination of each subsample. $(\alpha_{\text{sub}}, M_{\text{sub},1}^*)$ denoted the fitting parameter of LF for each sub-sample, and $M_{\text{sub},2}^*$ are fitting values of characteristic magnitude when we fixed the slope parameter to be the average value of 15 sub-samples, $\langle\alpha_{\text{sub}}\rangle$.

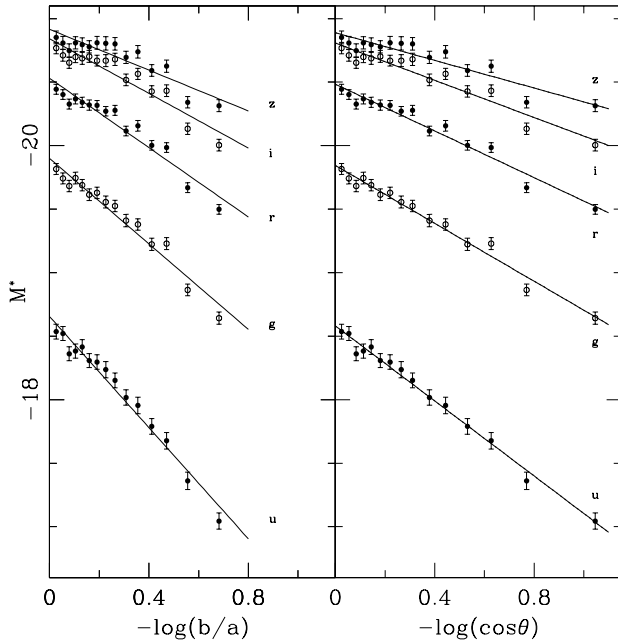


FIG. 7.— The inclination-dependence of M^* ($M_{\text{sub},2}^*$ listed in table 3, see text for details) and its best linear fit. Solid and open circles are used to distinguish two successive wave-bands.

4. INTERNAL DUST EXTINCTION

Having shown that the LF of spiral galaxies depends systematically on the inclination, we now model such dependence in terms of dust extinction.

4.1. Empirical extinction models

As a simple model for the dust extinction, we assume that the change in magnitude of a galaxy, ΔM , due to dust extinction is proportional to $\log(b/a)$, so that

$$\Delta M_1(b/a) = M(b/a) - M_1(1) = -\gamma_1 \log(b/a), \quad (9)$$

where γ_1 parameterizes the amplitude of the dust extinction relative to the face-on value (e.g. Giovanelli et al. 1994; Masters, Giovanelli & Haynes 2003). As discussed in § 2.2, a quantity that may better describe the inclination is the *corrected* cosine of the inclination angle, $\cos \theta$. We therefore consider another model in which

$$\Delta M_2(\cos \theta) = M(\cos \theta) - M_2(1) = -\gamma_2 \log(\cos \theta). \quad (10)$$

In the above expressions, the subscripts, ‘1’ and ‘2’ denote quantities in the two models. Note that $M_1(1)$ and $M_2(1)$ are the magnitudes corresponding to $b/a = 1$ and $\cos \theta = 1$, i.e. face-on disk.

Since the inclination-dependence of α_{sub} is not strong, the main effect of dust extinction is to change M_{sub}^* . The change of M_{sub}^* with inclination may be used to infer the average dust extinction for all spiral galaxies in the sample. The results of the least square fits of equations (9) and (10) to the observed $M_{\text{sub},2}^* - \log(b/a)$ and $M_{\text{sub},2}^* - \log(\cos \theta)$ relations are shown in Fig. 7, while the values of the best fit γ and $M^*(1)$ are listed in Table 4 along with the corresponding χ^2 values. There is significant difference between the results based on the apparent

TABLE 4
FITTING PARAMETERS OF THE LINEAR RELATIONSHIP BETWEEN M^* AND THE LOGARITHMIC OF THE INCLINATION. ALSO SEE SOLID LINES IN FIGURE 7.

Band	$M_1^*(1)$	γ_1	χ_1^2	$M_2^*(1)$	γ_2	χ_2^2
u	-18.65 ± 0.03	2.19 ± 0.08	18.82	-18.58 ± 0.02	1.48 ± 0.06	7.24
g	-19.90 ± 0.02	1.68 ± 0.06	31.36	-19.84 ± 0.02	1.14 ± 0.04	15.31
r	-20.53 ± 0.02	1.37 ± 0.05	48.28	-20.48 ± 0.02	0.92 ± 0.04	26.29
i	-20.84 ± 0.02	1.08 ± 0.06	41.61	-20.81 ± 0.02	0.73 ± 0.04	26.77
z	-20.92 ± 0.02	0.80 ± 0.07	30.98	-20.89 ± 0.02	0.54 ± 0.04	23.71

axis ratio b/a and those based on the corrected inclination angles θ . For all of the 5 wave bands, $\chi_2^2 < \chi_1^2$, suggesting that a linear model works better for the corrected inclination angle. The values of γ_2 are all smaller than γ_1 , because the relation between b/a and $\cos \theta$ has a slope that is different from 1 (see Figure 3). However, the ratios between the γ values in different wave bands are quite similar in the two models. As we will see in § 4.2, it is these ratios that describe the dust extinction curve. In the maximum-likelihood estimate of the LF used here, dust extinction can be incorporated in a more elegant way. Since equation (10) provides a reasonable description of the mean relation between the dust extinction and the inclination angle θ , a similar relation may be used for individual galaxies. In this case, the luminosity function of spiral galaxies with observed luminosity L and inclination angle θ can be parameterized by

$$\phi(L, \theta) \propto [(L/L^*)(\cos \theta)^{-0.4\gamma}]^\alpha \exp [-(L/L^*)(\cos \theta)^{-0.4\gamma}], \quad (11)$$

Thus, the value of γ (assumed to be independent of galaxy luminosity) can also be determined through the maximum likelihood method (either the STY method or the SWML method) that determines the LF. We have carried out such a maximum likelihood analysis using the STY method. Again, an iterative procedure is used so that only galaxies with luminosities in the range between $M^* + 3.5$ and $M^* - 2.0$ are used in the fitting. Since $\cos \theta$ for individual galaxies are obtained statistically from Monte-Carlo simulations, different realizations may give different results. We therefore construct 25 different realizations and obtain the values of α , M^* and γ for each of them. The average values of α , M^* and γ obtained in this way are listed in Table 5 as α_0 , M_0^* and γ_3 , where the subscript ‘0’ is used to denote ‘face-on’ galaxies, and the subscript ‘3’ in γ_3 is used to distinguish it from γ_1 and γ_2 obtained from the $M_{\text{sub},2}^* - \log(b/a)$ relation and the $M_{\text{sub},2}^* - \log(\cos \theta)$ relation. The uncertainties on these parameters include both fitting errors and the scatter among the 25 realizations. The error bars are all very small, because each sample is sufficiently large to represent the distribution of $\cos \theta$ faithfully. Note that the values of γ_3 are similar to that of γ_2 , indicating that the method based on M^* and that on individual galaxies give the same results.

4.2. Extinction curves

The wavelength-dependence of γ can be used to constrain the extinction curve for spiral galaxies. As a simple model, we assume that the effective extinction curve in

TABLE 5
CORRECTED LUMINOSITY FUNCTION (EQ. 11) FOR SPIRAL
GALAXIES IN EACH OF THE SDSS BAND

Band	N_{spiral}	α_0	M_0^*	γ_3
<i>u</i>	23380	-1.28 ± 0.02	-18.60 ± 0.02	1.59 ± 0.05
<i>g</i>	42150	-1.22 ± 0.01	-19.89 ± 0.01	1.24 ± 0.03
<i>r</i>	60100	-1.25 ± 0.01	-20.54 ± 0.01	0.92 ± 0.02
<i>i</i>	51290	-1.28 ± 0.01	-20.87 ± 0.01	0.80 ± 0.02
<i>z</i>	42820	-1.26 ± 0.01	-20.96 ± 0.01	0.65 ± 0.03

. These values represent the parameters for pure face-on spiral galaxies.

TABLE 6
FITTING RESULTS FOR THE EXTINCTION CURVE (EQ. 13).

	γ_V	n	χ^2
Case 1 (using γ_1)	1.45 ± 0.02	0.97 ± 0.07	3.94
Case 2 (using γ_2)	0.98 ± 0.02	0.97 ± 0.07	3.71
Case 3 (using γ_3)	1.05 ± 0.01	0.96 ± 0.04	1.50

the optical has a power-law form,

$$\tau_\lambda(\cos \theta) = \tau_V(\cos \theta)(\lambda/5500\text{\AA})^{-n}, \quad (12)$$

where λ is the wavelength, τ_λ is the optical depth at λ , τ_V is the optical depth at the *V*-band (centered at $\lambda = 5500\text{\AA}$) and is a function of inclination angle, and n is the power index describing the shape of the dust extinction curve. If we neglect the difference in the dust extinction curve for different galaxies and compare the dust extinction at given inclination angle but in different wavelength, then γ is proportional to τ . Thus, we can write

$$\gamma_\lambda = \gamma_V(\lambda/5500\text{\AA})^{-n}, \quad (13)$$

where γ_V is the value of γ at 5500\AA .

We use a least-square fitting to estimate γ_V and n from the values of γ in the 5 SDSS bands, and the results are listed in Table 6 for the three cases, Cases 1, 2 and 3, corresponding to the use of γ_1 , γ_2 and γ_3 , respectively. In Figure 8, we plot the fitting results along with the data of γ used in the fit. As one can see, the power-law model is a good assumption in all cases. It is also interesting to note that, although the values of γ_1 , γ_2 and γ_3 are different, the power-law indices obtained from them are very similar, with $n = 0.96 \pm 0.04$. (12) we obtained from the SDSS data are extrapolated to the near-infrared, and compared with the data obtained by Masters et al. (2003) for spiral galaxies with $\log(a/b) < 0.5$ in the 2MASS: $\gamma_J = 0.48 \pm 0.15$, $\gamma_H = 0.39 \pm 0.15$ and $\gamma_{K_s} = 0.26 \pm 0.15$. In addition, we also plot results obtained by others in various bands. Tully et al. (1998) gave $\gamma_B = 1.0 - 1.5$ for different types of spiral galaxies. Courteau (1996) obtained $\gamma_{r_{\text{Gunn}}} = 0.95$ using 349 Sb-Sc UGC galaxies with $0.27 < \log(a/b) < 0.70$. Han (1992) found γ_I to be in the range from 0.51 to 0.91 for different types of galaxies in the *I* band. Finally, Giovanelli et al. (1994) obtained $\gamma_I = 0.95 - 1.15$. Remarkably, all of the results follow well the power-law we obtained from the SDSS data.

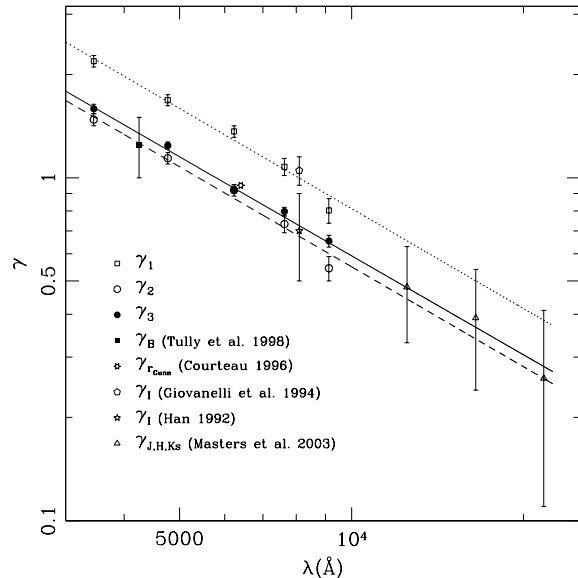


FIG. 8.— The best fit of the extinction curve in optical wavebands. The values of γ are those given by the different methods described in § 4.2. Data points show the values of γ obtained by other investigators.

It should be pointed out, however, that the dust extinction we obtained here is the effective extinction for an entire galaxy, rather than that from some specific regions within a galaxy. Such extinction depends not only on the properties of the dust grains but also on the distribution of dust in individual galaxies. The index, $n = 0.96 \pm 0.04$, obtained is shallower than that obtained by observations of the Milky Way, the LMC and the SMC, $n = 1.1 - 1.5$, but steeper than the value $n = 0.7$ obtained by Charlot et al. (2000) based on the assumption that dust in a spiral galaxy has a patchy distribution. Our result of $n \sim 1$ implies that dust distribution in spiral galaxies on average are not as patchy as assumed in Charlot et al. (2000).

5. EXTINCTION-CORRECTED LUMINOSITY FUNCTION

5.1. Luminosity-dependence of extinction

In the analysis presented above, we have assumed that the value of γ is independent of luminosity. In this subsection we examine whether or not this assumption is valid. To do this, we consider a model in which γ is a linear function of the magnitude,

$$\gamma(M) = \gamma^*[1 + \beta(M - M^*)]. \quad (14)$$

We treat β as the fourth free parameter in fitting the LF. The result shows that β has a very small value so that the difference between γ and γ^* is less than 5%. Furthermore, if α is kept constant in the fitting, β is even smaller. Thus, the luminosity-dependence of γ is weak and will be neglected in the following. Note, however, that γ in our definition only characterizes the extinction at a given inclination relative to that of face-on galaxies. Thus, even if γ is independent of galaxy luminosity, the absolute value of the extinction may be luminosity-dependent, if the extinction of face-on galaxies depends on luminosity. Unfortunately our method,

which is based on a comparison between inclined galaxies with face-on galaxies, cannot be used to obtain the absolute value of the extinction. Because of this, here we use an independent set of observational data to probe the luminosity-dependence of extinction and to examine how such data can be used together with our results to obtain an extinction-corrected luminosity function for spiral galaxies.

Kauffmann et al. (2003) estimated the dust extinction in the SDSS z -band, A_z , for galaxies in the SDSS DR2, using the 4000\AA break strength and the Balmer absorption line index $H\delta_A$ to constrain the star formation history and then estimating the dust extinction from the difference between the model and observed $g-r$ and $r-i$ colors. We combine their data with our sample. It should be noted that the 4000\AA breaks and the $H\delta_A$ indices are estimated from the SDSS fiber spectra within a 3-arcsec aperture. Thus, the values of A_z given by Kauffmann et al. may be biased towards the central parts of galaxies, especially for nearby galaxies with large apparent sizes. Figure 9 shows A_z versus luminosity for galaxies in our sample. The small dots in the upper panel show all galaxies in the ‘face-on’ subsample with $0.86 < b/a < 0.91$. Open circles with error bars represent the median and their errors within given bins of M_z . As a comparison, the solid circles show the median values of A_z for ‘edge-on’ galaxies with $0.25 < b/a < 0.31$. The solid circles are shifted by 0.5 magnitude towards the bright end according to the difference in M_{sub}^* for these two subsamples. It is clear that dust extinction does depend on luminosity for both face-on and edge-on galaxies. The dependence is not a simple monotonic relation. The extinction increases with luminosity at the faint part and decreases slightly towards the bright end. The behavior at the faint end may indicate that the dust opacity is larger in brighter galaxies. The slight decrease of A_z with luminosity at the bright end may be due to the fact that the contribution of the central bulge, which may be less dusty, becomes more important for brighter galaxies. Note that the mean A_z - M_z relation for the face-on subsample is roughly parallel to that for the edge-on subsample, except perhaps for faint galaxies (see the lower panel of Figure 9). Since $\gamma_z \propto \Delta A_z$, this result implies that γ_z is quite independent of luminosity, consistent with our result based on the luminosity functions.

The difference in A_z between face-on and edge-on galaxies is about 0.4 magnitude, in good agreement with the difference in M_{sub}^* (0.5 mag) between these two subsamples. We have also checked the M_z -dependence of A_z for other subsamples of b/a , and found that the relations are all roughly parallel to each other, with the relative amplitudes very similar to those obtained from fitting the LFs (see Table 3). This agreement is remarkable, because the A_z values given by Kauffmann et al. (2003) are based on totally different considerations.

5.2. Extinction-corrected luminosity function

5.2.1. Luminosity function of face-on galaxies

Based on the results presented above, we can have several estimates for the LF of face-on spiral galaxies. The first one is based on $(\alpha_{\text{sub}}, M_{\text{sub},1}^*)$, or, $(\langle\alpha_{\text{sub}}\rangle, M_{\text{sub},2}^*)$, obtained from the subsamples with big values of axis ratio (see lines 14 and 15 in Table 3). The second is given

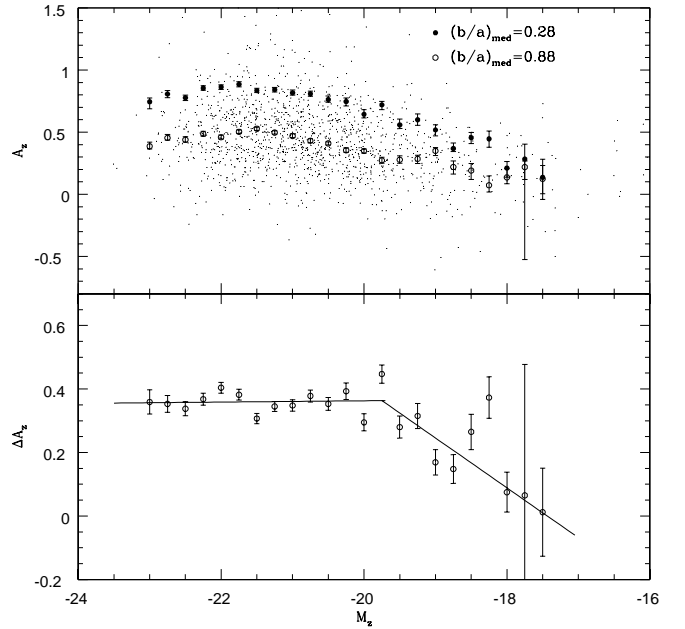


FIG. 9.— The luminosity-dependence of the dust extinction in the z -band (A_z). In the upper panel, small dots are the values of A_z obtained by Kauffmann et al. (2003) for individual face-on spiral galaxies with $0.86 < b/a < 0.91$. Open circles with error bars represent the median value of A_z for a given M_z . Solid circles are the same as open ones but for galaxies with $0.25 < b/a < 0.31$ (almost edge-on). The lower panel shows the difference of A_z between face-on and edge-on galaxies. Solid lines here show a fitting by eye of the data points.

by $(\langle\alpha_{\text{sub}}\rangle, M_1^*(1))$ or $(\langle\alpha_{\text{sub}}\rangle, M_2^*(1))$, where $M_1^*(1)$ and $M_2^*(1)$ are the values of M^* for face-on galaxies obtained from fitting the M_{sub}^* -inclination relations (see Table 4). The most rigorous estimate may be given by the values of (α_0, M_0^*) in Table 5, obtained through the maximum likelihood analysis that includes γ as the 3rd parameter (eq. 11). Note that for all the 5 SDSS bands, the values of $\langle\alpha_{\text{sub}}\rangle$ and α_0 are similar, but both are slightly less negative than α_{obs} , the faint end slope of directly measured LF of spirals (§ 3.2). Furthermore, unlike α_{obs} , which has more negative values in the bluer bands, both $\langle\alpha_{\text{sub}}\rangle$ and α_0 are quite independent of wavebands. This may be explained by the fact that dust extinction not only reduces L^* , but also steepens the LF for spiral galaxies. We have tested this effect using a Monte Carlo simulation. We generated a sample of galaxies with a given LF, and with each galaxy assigned a random orientation. We then made each galaxy dimmer according to its inclination angle. We found that the resulting LF is steeper than the original LF.

The corrections in the characteristic magnitudes are also significant. For face-on galaxies, $M_1^*(1)$, $M_2^*(1)$ and M_0^* are all brighter than M_{obs}^* for about 0.2-0.3 magnitudes. Figure 10 shows a comparison of M^* s for all the 5 bands. According to the extinction curve ($\tau \propto \lambda^{-1}$), the change in M^* is expected to be larger for bluer band. That such dependence is not seen clearly in Figure 10 is largely caused by the change in α and the degeneracy between α and M^* .

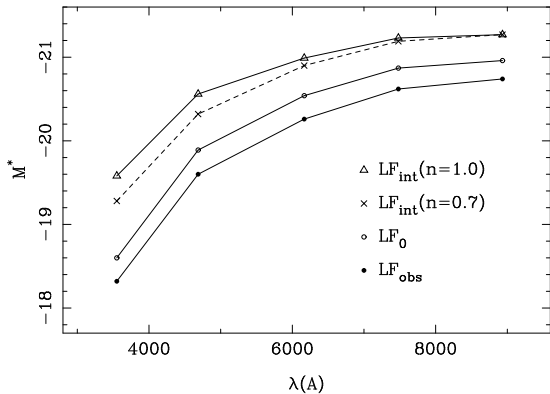


FIG. 10.— A comparison between the values of M^* obtained from different cases in different bands. LF_{obs} labels the results of the observational sample without any dust correction. LF_0 labels the results for face-on galaxies obtained by correcting the inclination effects. LF_{int} labels the results for ‘extinction-corrected’ luminosity functions.

5.2.2. Intrinsic Luminosity Function

According to Figure 9, the values of A_z for face-on galaxies are typically 0.3-0.4 magnitudes. In principle, we can use the values of A_z for individual galaxies and estimate a dust-corrected LF. The LFs in other bands can also be obtained using the dust extinction curve. Unfortunately, this approach is impractical, because the uncertainty in A_z is quite large ($\Delta A_z \geq 0.2$) and can significantly broaden the LF. On the other hand, for galaxies with a given luminosity, the true values of A_z may have intrinsic scatter, which should be taken into account in the dust correction. Because of this uncertainty, here we consider two extreme cases. In one, we use the A_z values given by Kauffmann et al. (2003) to make correction for each galaxy, and estimate the LF for the ‘corrected’ sample. The LF parameters obtained in this way are $\alpha = -1.43 \pm 0.01$ and $M^* = -21.52 \pm 0.01$. In the second case, we average the values of A_z for galaxies with similar inclination angles, and use them to correct individual galaxies. The LF parameters obtained in this way are $\alpha = -1.28 \pm 0.01$ and $M^* = -21.27 \pm 0.01$. As discussed above, the true LF is expected to be between these two. Our Monte Carlo simulation showed that the uncertainty in A_z , about 0.2, can account for most of the difference between these two results. So the second estimation of LF may close to the real case.

For the other 4 bands, direct estimates of the dust extinction are not available. We therefore use an assumption of the dust extinction curve together with the average values of A_z (as a function of b/a) to make dust corrections for individual galaxies. We list the parameters for the LFs obtained for the corrected samples in Table 7 as α_{int} and M_{int}^* . For comparison, results are given for two extinction curves, one with $n = 1.0$, as is obtained in this paper, and the other is $n = 0.7$, as given in Charlot et. al. (2000).

In Figure 10, we plot M^* in all the five bands for different cases: the directly observed LF, the LF for face-on galaxies, and the intrinsic LFs obtained above. It is clear that the differences between different cases are quite large. In particular, M^* for the corrected LF could be 0.5-1.2 magnitudes brighter than the uncorrected one

TABLE 7
PARAMETERS OF LUMINOSITY FUNCTION FOR SPIRAL GALAXIES
WITH CORRECTION OF DUST EXTINCTION.

Band	n=1.0			n=0.7		
	N_{spiral}	α_{int}	M_{int}^*	N_{spiral}	α_{int}	M_{int}^*
<i>u</i>	22887	-1.46±0.01	-19.58±0.02	22902	-1.50±0.01	-19.28±0.02
<i>g</i>	41587	-1.32±0.01	-20.56±0.01	41582	-1.32±0.01	-20.32±0.01
<i>r</i>	59545	-1.26±0.01	-20.99±0.01	59536	-1.26±0.01	-20.90±0.01
<i>i</i>	50718	-1.30±0.01	-21.23±0.01	50719	-1.30±0.01	-21.19±0.01
<i>z</i>	42311	-1.28±0.01	-21.27±0.01	42311	-1.28±0.01	-21.27±0.01

from *z* to *u* bands. This suggests that, without correcting internal extinction of galaxies, the L^* for spiral galaxies can be seriously under-estimated.

6. SUMMARY AND DISCUSSION

Using a samples of 61506 spiral galaxies selected from the SDSS DR2, we study the luminosity functions of spiral galaxies with different inclination angles. The apparent axis ratio, b/a , is used as an observational inclination indicator to define subsamples of spiral galaxies at different inclinations, and we use a Monte Carlo process to connect b/a to the corrected inclination angle, θ , disk thickness, ν , and ellipticity ϵ . There is a systematic change of the LF with inclination angle: the characteristic luminosity L^* decreases with increasing inclination angle, while the faint-end slope depends only weakly on inclination.

The inclination-angle dependence of the galaxy luminosity function is consistent with the expectation of a simple model where the optical depth is proportional to $\cos \theta$, and we use a likelihood method to recover both the amplitude of the extinction (relative to the face-on value), γ , and the luminosity function for galaxies viewed face-on. We found that the results obtained from different methods are all consistent with each other, and the characteristic magnitude for face-on spirals is about 0.2 ~ 0.3 magnitudes brighter than the average population.

We found that the value of γ is quite independent of luminosity in a given band. The values of γ obtained in this way for the 5 SDSS bands are used to constrain the shape of the extinction curve, assuming $\tau_\lambda = \tau_V(\lambda/5500\text{\AA})^{-n}$. We find $n = 0.96 \pm 0.04$.

Using the *z*-band dust extinction given by Kauffmann et al. (2003), together with the inclination-dependence of the LF we obtained, we derive an ‘extinction-corrected’ luminosity function for spiral galaxies. Dust extinction makes a significant change in M^* , and the characteristic luminosity of the ‘dust-corrected’ LF is about 0.5 to 1.2 magnitude brighter than the uncorrected LF from the *z*- to the *u*-bands. This suggests that the luminosity function of spiral galaxies may be significantly underestimated in blue bands, if internal dust correction is not made. This may have important implications when comparing model predictions of the luminosity function with observations.

As mentioned in the introduction, the dimming in luminosity from face-on to edge on is expected if galaxy disks are optically thick. Our results therefore give support to the assumption that most of the disks in our galaxy sample are optically thick. Note that the

inclination-dependent dimming exists not only for faint galaxies but for galaxies over the entire luminosity range. Note also that we are using a well-defined flux-limited sample and the selection bias is taken into account in the LF estimate. It is therefore unlikely that the effect we find here is due to the magnitude limit in the sample. Systematic effects of surface brightness relative to the inclination is also unlikely to play an important role here. As discussed in Blanton et al. (2001), the surface-brightness limit used in the SDSS has negligible effects on the LF at $M_r < -18$, and so the inclination-dependence of the LF at $M_r < -18$ cannot be explained as due to the miss of low-surface face-on galaxies. We therefore conclude that our results are best explained by assuming that bright disks are optically thick.

The authors thank Shude Mao, Jiasheng Huang, Chenggang Shu, Ruixiang Chang for their valuable advice and discussion. Thanks are also due to the anonymous referee for helpful comments. This research was

supported by NSF of China grants No. 10273016, 10333060, and also supported in part by the National Science Foundation under Grant No. PHY99-07949.

Funding for the creation and distribution of the SDSS Archive has been provided by the Alfred P. Sloan Foundation, the Participating Institutions, the National Aeronautics and Space Administration, the National Science Foundation, the U.S. Department of Energy, the Japanese Monbukagakusho, and the Max Planck Society. The SDSS Web site is <http://www.sdss.org/>. The SDSS is managed by the Astrophysical Research Consortium (ARC) for the Participating Institutions. The Participating Institutions are The University of Chicago, Fermilab, the Institute for Advanced Study, the Japan Participation Group, The Johns Hopkins University, Los Alamos National Laboratory, the Max-Planck-Institute for Astronomy (MPIA), the Max-Planck-Institute for Astrophysics (MPA), New Mexico State University, Princeton University, the United States Naval Observatory, and the University of Washington.

REFERENCES

- Abazajian, K. et al. 2004, *AJ*, 128, 502
 Bernardi, M. et al., 2005, *AJ*, 129, 61
 Binney, J. et al., 1985, *MNRAS*, 212, 767
 Blanton, M.R. et al., 2001, *AJ*, 121, 2358
 Blanton, M.R. et al., 2005, *AJ*, 129, 2562
 Burstein, D.; Haynes, M.P.; Faber, M., 1991, *Natur.*, 353, 515
 Byun, Y., 1993, *PASP*, 105, 993
 Calzetti, D. 2001, *PASP*, 113, 1449
 Charlot, S., Fall, S.M. 2000, *ApJ*, 539, 718
 Courteau, S. 1996, *ApJS*, 103, 363
 Efstathiou, G., Ellis, R.S., & Peterson, B.A., 1988, *MNRAS*, 232, 431
 Giovanelli, R., Haynes, M., Salzer, J.J., Wegner, G., da Costa, L.N., & Freudling, W. 1994, *AJ*, 107, 2036
 Giovanelli, R., Haynes, M., Salzer, J.J., Wegner, G., da Costa, L.N., & Freudling, W. 1995, *AJ*, 110, 1059
 Han, M. 1992, *ApJ*, 391, 617
 Holmberg, E. 1958, *Medde. Lunds Astron. Obs., Ser. II*, 136, 1
 Holmberg, E. 1975, in *Stars and Stellar Systems, Vol. IX*, edited by A. Sandage, M. Sandage and Kristian, Chap. 4., p. 123
 Holwerda, B.W., Gonzalez, R.A., Allen, R.J., & van der Kruit P.C., 2005, *AJ*, 129, 1396
 Kauffmann G., Heckman T.M., White S.D.M., et al., 2003, *MNRAS* 341, 54
 Masters, K.L., Giovanelli, R., & Haynes, M.P., 2003, *AJ*, 126, 158
 Nakamura, O., Fukugita, M., Yasuda N., Loveday J., Brinkmann, J., Schneider D.P., Shimasaku, K.; SubbaRao, M., 2003, *AJ*, 125, 1682
 Petrosian V., 1976, *ApJ*, 209, L1
 Ryden B.S., 2004, *ApJ*, 601, 214
 Sandage, A., Tammann, G.A., & Yahil, A., 1979, *ApJ*, 232, 352
 Schechter, P. 1976, *ApJ*, 203, 297
 Schlegel D.J., Finkbeiner D.P., Davis M., 1998, *ApJ*, 500, 525
 Shen, S., et al. 2003, *MNRAS*, 343, 978
 Stoughton, C., et al. 2002, *AJ*, 123, 485
 Tully, R.B., Pierce, M.J., Huang, J-S., Saunders, W., Verheijen, M. A. W., & Whichalls, P. L., 1998, *AJ*, 115, 2264
 Xilouris, E. M., Byun, Y. I., Kyllafis, N. D., Paleologou, E. V., Papamastorakis, J. 1999, *AA*, 344, 868
 York D. et al., 2000, *AJ*, 120, 1579